Understanding the Visible Light Initiated Manganese Catalyzed Synthesis of Quinolines and Naphthyridines under Ambient and Aerobic Conditions

Kamaless Patra,[‡†] Arindom Bhattacherya,[†] Chenfei Li,[‡] Jitendra K. Bera,*[†] and Han Sen Soo*[‡]

[‡]School of Chemistry, Chemical Engineering and Biotechnology, Nanyang Technological University, Singapore, 21 Nanyang Link, Singapore 637371, Singapore.

E-mail: hansen@ntu.edu.sg

[†]Department of Chemistry and Centre for Environmental Science and Engineering, Indian Institute of Technology Kanpur, Kanpur 208016, Kanpur, India

E-mail: jbera@iitk.ac.in

KEYWORDS: photoinitiated catalysis, manganese complexes, quinolines, naphthyridines, aerobic oxidation, visible light

ABSTRACT: Polyaromatic *N*-heterocycles are some of the most common building blocks in natural products and active pharmaceutical ingredients. Significant efforts have been devoted to develop catalytic protocols, including those which use an acceptorless dehydrogenation strategy at elevated temperatures, to produce polyaromatic *N*-heterocycles like quinolines and naphthyridines. However, photoinitiated catalysis driven by visible light offers a milder and often more selective protocol as an alternative to thermal reactions. Here, we present the catalytic syntheses of quinolines and naphthyridines from *ortho*-aminobenzyl alcohols and ketones using the photocatalyst $[Mn(L^1H)(CO)_3Br]$ (L^1H = 7-hydroxy-2-methyl-1,8-naphthyridine-*N*-oxide), bearing a phenolic unit on a 1,8-naphthyridine-*N*-oxide scaffold, under ambient and aerobic conditions with visible light illumination. We describe a broad, functional group-tolerant substrate scope of >30 examples under modest reaction conditions. A variety of 2-aminobenzyl alcohols containing electron-donating and electron-deficient groups and (2-aminopyridin-3-yl)methanol are converted to the corresponding quinolines and naphthyridines using ambient air as an oxidant in the presence of KOH. We synthesized a wide range of derivatives, including some of the bioactive antimalarial drug chloroquine and the steroids progesterone and pregnenolone to highlight the value-added applications of this catalytic protocol for pharmaceutical ingredient and natural product syntheses. We performed substrate viability, UV-visible, EPR, and XPS studies, as well as DFT calculations to gain mechanistic insights to the reaction pathway. The catalytic cycle involves condensation of the amino group in the *ortho*-aminobenzyl alcohol with the ketone initially, which is followed by aerobic oxidation of the benzyl alcohol to the corresponding benzaldehyde catalyzed by the photoinitiator $[Mn(L^1H)(CO)_3Br]$ in the presence of visible light, and finally, a KOH-promoted condensation and cyclization to afford quinolines as the final products.

INTRODUCTION

Polyaromatic *N*-heterocycles are ubiquitous in natural products and active pharmaceutical ingredients (APIs) owing to their Lewis basicity and bioactivity. An earlier survey of APIs approved by the United States Food and Drug Administration revealed that around 59% of the approved drug molecules contained a nitrogen heterocycle, of which six-membered heterocycles like piperidine, pyridine, and piperazine are the most common.[1] Polyaromatic heterocycles such as naphthyridines are interesting owing to their enzyme inhibition,[2,3] antibacterial,[4] and antioxidant properties,[5] while quinolines have featured as anticancer agents, enzyme inhibitors, and antimalarial drugs.[1,6–13] Quinolines have an especially long history for antimalarial activity since quinine was isolated from the alkaloid mixture extracted from the bark of the Chinchona tree, which subsequently led to the development of many synthetic quinoline derivatives those operate with distinct molecular pharmacologies (Figure 1).[12,13]

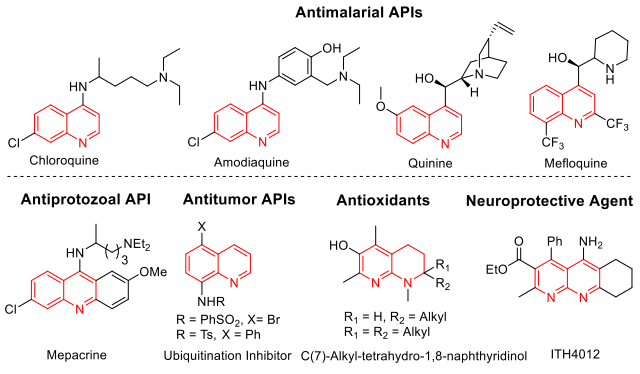

Figure 1. Examples of APIs and natural products featuring quinoline scaffolds.

Because of the perennial and escalating problem of emerging strains of the *P. falciparum* parasites that are resistant

to chloroquine and other quinine derivatives,[12,13]it is imperative that protocols which are general, sustainable and affordable are readily available to access quinoline derivatives.

Traditionally, the synthesis of quinolines and other polyaromatic *N*-heterocycles have relied on the Friedländer reaction via acid- or base-catalyzed thermal condensation of 2-aminobenzaldehydes or 2-aminophenylketones with another carbonyl compound containing acidic α-methylene protons.[14] Of late, despite its long history, greener and milder procedures continue to be developed for the Friedländer reaction,[14–19] underscoring the importance of these *N*-heterocycles in medicinal applications. The precursor 2-aminobenzaldehydes and their congeners are notoriously unstable and polymerize by condensation reactions at room temperature, which necessitates their storage at lower temperatures. Consequently, there has been significant interest in accessing quinolines, naphthyridines, and related polyaromatic *N*-heterocycles from 2-aminobenzyl alcohols, which are more stable and are usually cheaper as feedstocks. There have been a number of recent reports on dehydrogenative strategies to couple 2-aminobenzyl alcohols with ketones or nitriles,[20–26] including those involving acceptorless dehydrogenation processes.[27–37] However, all these reactions typically require elevated temperatures above 80 ºC, which is detrimental to thermally sensitive and readily oxidizable functional groups like amines. Moreover, the H_2 gas liberated during the acceptorless dehydrogenation reactions is not recovered for any practical purpose and the reactions have to be performed under inert atmospheres,[27–37] thus diminishing their value and operational convenience relative to reactions that can just be carried out by aerobic oxidation.[7,38–42]

Over the past decade, there has been a renaissance in the use of light as the energy source instead of heat during photoredox catalysis to initiate reactions for organic synthesis, pioneered by the work of MacMillan, Fukuzumi, Yoon, and others.[43–53] Majority of the previous work have relied on photosensitizers based on expensive Pt group metals such as Ru and Ir because of their efficacy, but there has been growing interest in the application of the more earth-abundant and potentially less toxic first-row transition metals. For instance, there have been a growing number of papers on the use of molecular catalysts comprising V,[54–59] Cr,[60–62] Fe,[63] Co,[64–69] and Cu[70–74] for photoredox reactions.[75,76] However, examples of Mn in photocatalysis are scant. Some notable examples are Nam and Fukuzumi's seminal work on a high valent chiral Mn-oxo complex generated by photooxidation using $[Ru(bpy)_3]^{2+}$,[77] and a number of cases where CO complexes of Mn were photoactivated to mediate C-C bond formation reactions are reported (Figure 2a).[75,78–81] This is despite the fact that oxygen evolving Mn clusters form the backbone of redox catalysis in natural[82] and artificial[83] photosynthesis. There have also been a small number of instances where Mn complexes were employed for the synthesis of *N*-heterocycles at elevated temperatures (Figure 2b).[25,27,30,33,37,84]

Against this backdrop, our team has been working towards developing photocatalytic processes that include earth-abundant first-row or main group elements into artificial photosynthetic systems.[54–59,73,85–88] Here, we illustrate the use of Mn photocatalysts for the ambient and aerobic synthesis of quinolines and naphthyridines from aminobenzyl alcohol precursors (Figure 2c). We further demonstrate the applicability of this greener protocol for the convenient four-step synthesis of a derivative of the antimalarial drug chloroquine over the seven-step industrialized process.[89] Through substrate viability experiments, and identification of putative intermediates by UV-visible and EPR experiments, we propose a mechanism that involves condensation, visible light-induced oxidation, and cyclization processes under ambient conditions, which represents a rare example of Mn photocatalysis and an eco-friendly procedure to synthesize valuable polyaromatic *N*-heterocyclic compounds.

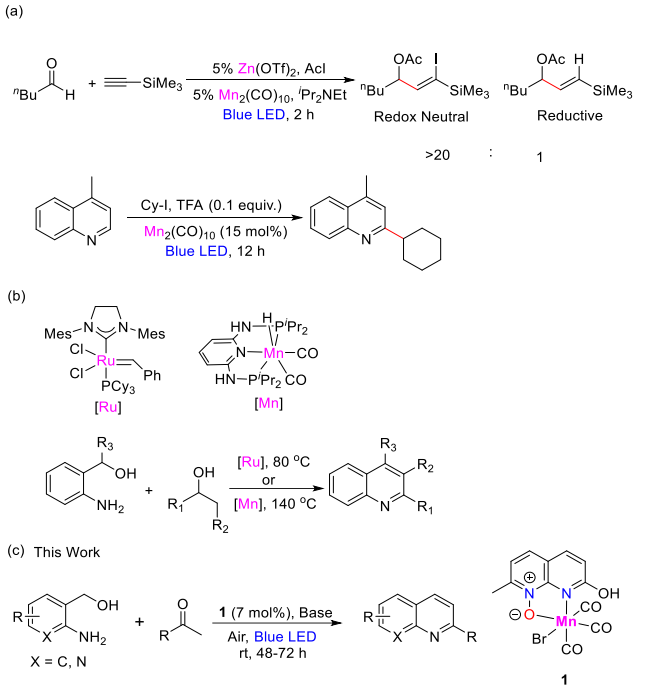

Figure 2 (a) Cross coupling reactions using the photoactivated carbonyl complex $Mn_2(CO)_{10}$ by Nagib,[80] and Fadeyi and Frenette.[78] (b) Synthesis of *N*-heterocycles via acceptorless dehydrogenative coupling using a Mn pincer and Ru catalyst at an elevated temperature by Kirchner[25] and Verpoort.[37] (c) This work.

RESULTS AND DISCUSSION

Syntheses of Mn complexes

We recently reported the complex $[Mn(L^1H)(CO)_3Br]$ (**1**), which was synthesized by the reaction of 7-hydroxy-2-methyl-1,8-naphthyridine-*N*-oxide ligand (**L^1H**) with $Mn(CO)_5Br$ in a 9:1 toluene/methanol solution for 4 h at 80 °C.[90]

Scheme 1. Synthesis of 2.

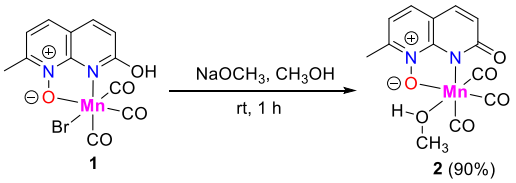

In addition, **1** was treated with one equivalent of sodium methoxide in methanol at room temperature for 1 h to afford **2** in 90% yield (Scheme 1). Both complexes were characterized by

^{1}H and ^{13}C NMR, which matches well with the previous report.[90]

Optimization of catalytic conditions and evaluation of substrate scope

The catalytic efficacy of **1** was investigated for the aerobic annulation of 2-aminobenzyl alcohol (**3a**) with ketones under visible light irradiation at room temperature. The utilization of 2-aminobenzyl alcohols over 2-aminobenzaldehydes provides a more cost-effective pathway and increases the selectivity by preventing undesired self-condensation side-products between the aniline and the benzaldehyde groups. We first explored the reaction of acetophenone with **3a** using 5 mol% of **1** and 1.5 equivalents of potassium hydroxide in toluene, but a yield of only 60% of 2-phenylquinoline (**4a**) was observed after 48 h (entry 1, Table 1).

Table 1. Screening of reaction conditions[a]

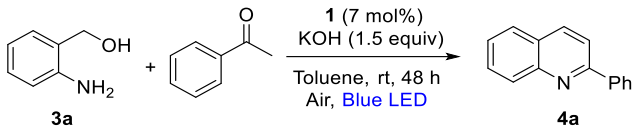

3a **4a**

Entry	Deviation from standard conditions	Yield (%)[b]
1	5 mol% of **1**	60
2	**none**	**82**
3	CsOH as base	45
4	KO^{t}Bu as base	65
5	K_2CO_3 or DABCO as base	nd[c]
6	*p*-xylene as solvent	75
7	THF, ACN, DCE or DMSO as solvent	<20
8	w/o **1** or Light	nd[c]
9	w/o air	5
10	$Mn(CO)_5Br$ instead of **1**	20

[a]Reactions were carried out using **3a** (0.100 mmol), acetophenone (0.100 mmol), base (0.150 mmol), and **1** (0.0070 mmol) at room temperature (rt) in 3 mL of solvent. Each reaction mixture was stirred in air under blue LED irradiation (50 W, emission maximum: 448 nm, full width at half maximum: 17.5 nm, see Supporting Information, Figure S1). [b]Yield was determined by GC–MS analysis using *n*–dodecane as an internal standard; [c]Not detected.

Further increase of the catalyst loading to 7 mol% raised the yield of **4a** to 82% with a turnover number (TON) of 11.7 (entry 2). Use of CsOH or KO^{t}Bu instead of KOH reduced the yields of **4a** to 45% and 65%, respectively (entries 3 & 4), whereas other bases (K_2CO_3, 1,4-diazabicyclo[2.2.2]octane (DABCO)) resulted in no detected amounts of **4a** (entry 5). The yield of **4a** reduced to 75% when *p*-xylene was used as the reaction solvent (entry 6), whereas acetonitrile, tetrahydrofuran, dimethyl sulfoxide, and dichloroethane all afforded considerably lower yields of **4a** (entry 7). Control reactions in the absence of either **1** or light resulted in the quantitative recovery of 2-aminobenzyl alcohol (entry 8). When the reaction was performed in the absence of air, a yield of only 5% of **4a** was observed (entry 9). A commonly used, commercially available Mn(I) precursor $Mn(CO)_5Br$ afforded lower yield (20%) under the optimized reaction conditions (entry 10). Here, the base is likely to play a number of roles. The KOH is needed for the ligand deprotonation, removal of the bromide from the metal, deprotonation of the benzyl alcohol substrate to the corresponding alkoxide, and condensation followed by cyclization of the putative 2-iminobenzaldehyde intermediate to afford corresponding quinoline **4a** (*vide infra*).

With the optimized conditions in hand, a range of ketones and **3a** were selected to showcase the functional group tolerance of our protocol (Figure 3).

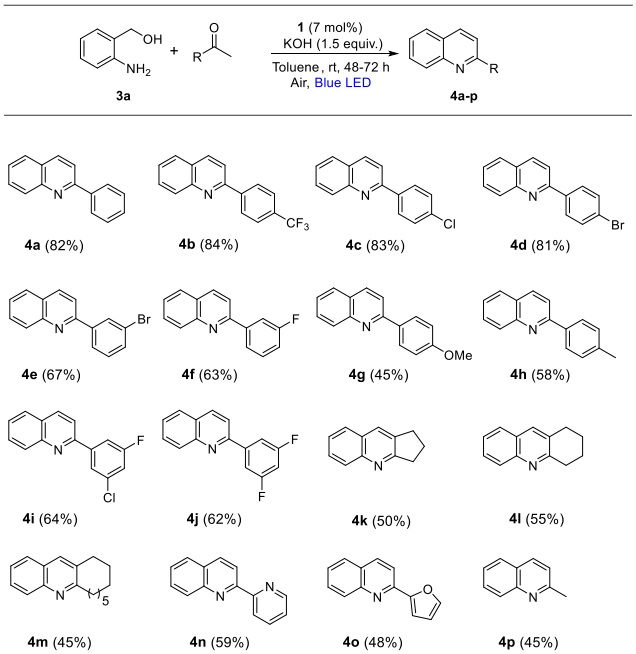

Figure 3. Scope of the reaction of **3a** with various ketones possessing different electron donor or acceptor abilities and functional groups. The reactions were carried out using **3a** (0.100 mmol), ketones (0.100 mmol), KOH (0.150 mmol), and **1** (0.0070 mmol) at room temperature in 3 mL of toluene. Each reaction mixture was stirred in air under blue LED irradiation (50 W). Isolated yields after purification are shown.

Acetophenone derivatives bearing electron-withdrawing substituents such as trifluoromethyl, fluoro, chloro, and bromo afforded **4b** to **4f** in good to moderate yields (84–63%, Figure 3) whereas electron-donating substituents like methoxy and methyl decreased the yields of **4g** and **4h** to 45% and 58%, respectively. The substrate scope for di-substituted acetophenones was also explored and their corresponding quinolines were obtained in moderate yields (64-62%, Figure 3, **4i** & **4j**). Furthermore, the use of aliphatic cyclic ketones provided **4k**-**4m** in moderate yields (45-55%, Figure 3). Heteroaromatic ketones like 2-acetylpyridine and 2-acetylfuran afforded **4n** and **4o** in moderate yields (59% and 48%, Figure 3). Use of the volatile aliphatic acetone furnished 2-methylquinoline (**4p**) in 45% yield.

The 2-aminobenzyl alcohols having an electron-donating methyl substituent *ortho* or *para* to the amino group were effectively transformed to **5a**-**5k** in excellent to moderate yields (88–

44%, Figure 4), while the electron-withdrawing chloro substituted 2-aminobenzyl alcohol afforded **5l** in a moderate 54% yield.

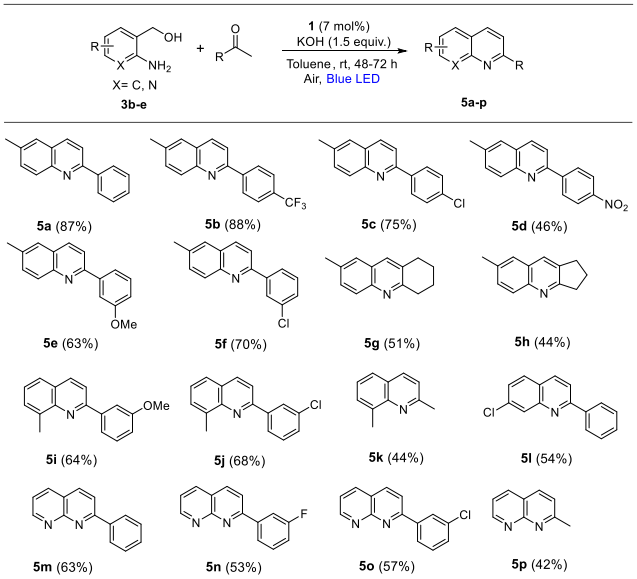

Figure 4. Scope of the reaction between substituted 2-aminobenzyl alcohols or (2-aminopyridin-3-yl)methanol with various ketones. The reactions were carried out using **3b-e** (0.100 mmol), ketones (0.100 mmol), KOH (0.150 mmol), and **1** (0.0070 mmol) at room temperature in 3 mL toluene. Each reaction mixture was stirred in air under blue LED irradiation (50 W). Isolated yields after purification are shown.

The use of acetone furnished 2,8-dimethylquinoline (**5k**) in 44% yield. Next, we evaluated the efficacy of **1** for the functionalization of (2-aminopyridin-3-yl)methanol (**3e**) to 1,8-naphthyridine derivatives. We conducted the reactions of **3e** with a series of electronically distinct aromatic and aliphatic ketones under the optimized conditions, which resulted in the formation of 1,8-naphthyridine derivatives in moderate yields (63-42%, **5m**-**5p**, Figure 4).

Functionalization of steroids

To demonstrate the versatility and value of our catalytic protocol, we applied it to the late-stage functionalizations of the bioactive steroids progesterone and pregnenolone, which possess carbonyl groups and have been investigated in structure activity relationship (SAR) and derivatization studies to realize their therapeutic potentials.[91–93]Progesterone and pregnenolone are widely used now for hormone replacement therapy. When the reaction with progesterone was carried out under the previously optimized conditions at room temperature, only the oxidation of 2-aminobenzyl alcohol to 2-aminobenzaldehyde occurred, but the annulation to the quinoline did not proceed well and only trace amounts of **6a** formed Upon slightly increasing the temperature to 45 °C, the yields improved dramatically and reached the levels observed in the simpler small molecule substrates. The use of 7 mol% of **1** and 1.5 equivalents of KOH at 45 °C in toluene afforded the corresponding quinoline derivatives of progesterone and pregnenolone (**6a**-**6c**) in 45–50% yields after 72 h (Scheme 2).

Scheme 2. Late-stage functionalization of progesterone and pregnenolone using 3a and 3c.

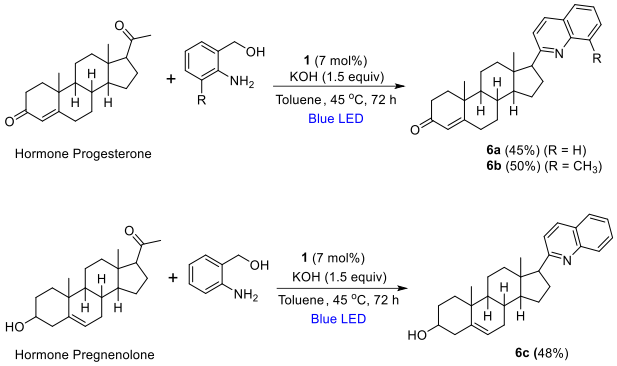

Synthesis of chloroquine derivative

The 4-aminoquinolines have been widely investigated for their pharmaceutical potential, especially their antimalarial properties.[12,13] Consequently, this scaffold is still of high interest for the development of novel antimalarial drugs. To highlight the applicability of our catalytic method for this objective, we achieved the synthesis of a chloroquine derivative in only four steps starting from **4p**, which was obtained by our protocol, and commercially available reagents (Scheme 3).

Scheme 3. Synthesis of the 4-aminoquinoline-based chloroquine derivative *N*,*N*-diethyl-*N*-(2-methylquinolin-4-yl)pentane-1,4-diamine (11).

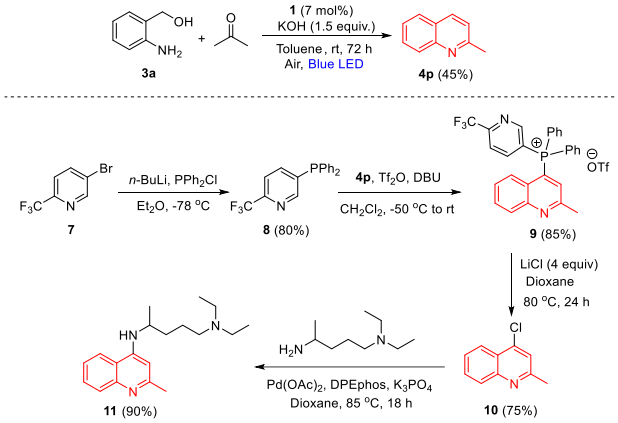

We performed the chlorination of **4p** at its 4-position using a known literature procedure utilizing a phosphine **8** as a nucleophile and a leaving group as well (Scheme 3).[94] In the first step, **8** was prepared by treating 2-trifluoromethyl-5-bromopyridine with chlorodiphenylphosphine in the presence of *n*-butyllithium at -78 °C, resulting in an 80% isolated yield of the product. In the next step, the reaction between **8** and **4p** was conducted at -50 °C in the presence of trifluoromethanesulfonic anhydride (Tf_2O) as an activating electrophile. After 1 h of stirring, 1,8-diazabicyclo[5.4.0]undec-7-ene (DBU) was added at -78 °C and the mixture was worked up in water to afford the phosphonium salt **9** in 85% yield. Further, a halide exchange reaction was performed with **9** using a common chloride salt, lithium chloride, as a nucleophile in dioxane. In the final step, C-N coupling of 4-chloro-2-methylquinoline (**10**) and the commercial 2-amino-

5-diethylaminopentane using another previously published procedure[95] with $Pd(OAc)_2$, DPEphos, and K_3PO_4 offered a mild and convenient pathway to afford the chloroquine derivative **11** from **4p**.

Mechanistic studies based on substrate viability experiments

A tentative mechanistic pathway for the formation of the quinoline from **3a** and a ketone involves the condensation of the amino group with a ketone first, followed by oxidation of the benzyl alcohol to benzaldehyde, and finally cyclization and aromatization in the presence of a base (Scheme 4).

Scheme 4. Proposed reaction pathway for quinoline formation

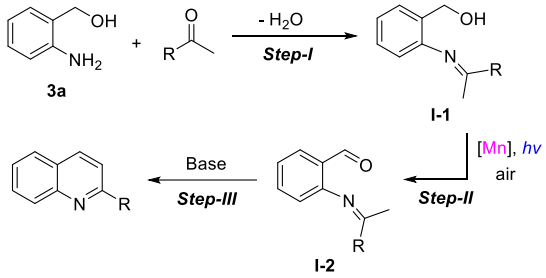

We performed additional substrate screening experiments to obtain deeper mechanistic insights for the multi-step photocatalytic reaction (Scheme 5). When we employed *N*,*N*-dimethylaminobenzyl alcohol (**12**) and acetophenone as the substrates under the standard optimized conditions, no reaction occurred and we quantitatively recovered both starting materials (Scheme 5a). We propose two possible reasons for this observation - i) condensation of the amine in **3a** with the ketone could be the first step followed by benzyl alcohol oxidation to benzaldehyde, which is not possible in the case of **12** as the substrate; or ii) oxidation of benzyl alcohol could be the first step in the catalytic reaction, which may be hindered by the presence of the bulky methyl groups of the NMe_2 present in the proximity of the alcohol unit.

Next, we also observed that under the standard optimized conditions in the absence of acetophenone, oxidation of **12** did not occur, whereas **3a** gave a 90% yield of the corresponding oxidized product, 2-amino-benzaldehyde (Scheme 5b and 5c). Both these experiments indicate that it is probably the steric factor arising from the -NMe_2 group that prevents the oxidation of **12**. Likewise, the use of acetaldehyde as a substrate instead of acetophenone along with **3a** did not furnish any product under the standard optimized conditions (Scheme 5d). The possible generation of a cyclic adduct (2-methyl-1,4-dihydro-2*H*-benzo[*d*][1,3]oxazine) could have been a reason for the lack of product formation.[96]

Further, when we repeated the same reaction in a single pot but in two steps, the formation of 2-aminobenzaldehyde from **3a** was observed in the first step, but the subsequent condensation and aromatization with acetaldehyde did not take place (Scheme 5e). The nucleophilicity of the amine in 2-aminobenzaldehyde is reduced significantly owing to the electron-deficient *ortho* aldehyde, which could be the reason why condensation with acetaldehyde did not occur. Based on these experiments, it is likely that condensation of the amine in **3a** with the ketone precedes alcohol oxidation. Otherwise, we should have observed quinoline as the product in both reactions with acetaldehyde.

Scheme 5. Substrate screening experiments for mechanistic understanding. a) Attempted reaction using the *N*,*N*-dimethyl substituted 12. b) Attempted photooxidation of 12. c) Photooxidation of the benzyl alcohol without ketone substrate. d) Attempted reaction using acetaldehyde instead of ketone. e) Attempted two-step reaction using acetaldehyde. f) Side-reaction using ethyl acetate as substrate.

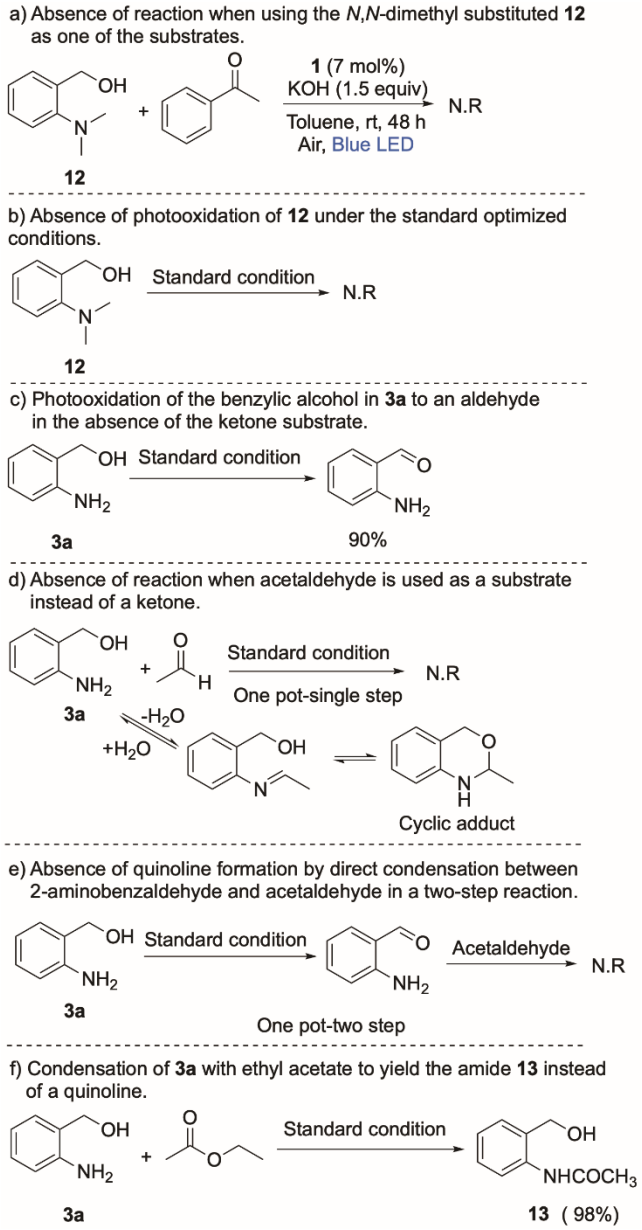

To confirm this hypothesis, we performed a reaction using ethyl acetate instead of a ketone that precludes a condensation. However, we observed the formation of *N*-(2-(hydroxymethyl)phenyl)acetamide **(13)** exclusively in 98% yield, formed likely via a nucleophilic substitution reaction (Scheme 5f). Since 2-aminobenzaldehyde was not observed even in a trace amount, an oxidation step could thus be ruled out. The experiments above together suggest a three-step formation of quinoline as follows: i) condensation of **3a** with a ketone to form the corresponding

imine intermediate **I-1**, which was detected by ESI-MS (m/z = 226.1219) using acetophenone and **3a** as substrates under the optimized reaction conditions in the absence of light (see Supporting Information, Figure S9); ii) coordination of **I-1** to the complex followed by Mn-catalyzed oxidation of **I-1** to the corresponding benzaldehyde species **I-2**; and III) the base-catalyzed aldol condensation followed by cyclization to afford the quinoline (Scheme 4).

Mechanistic studies based on observations of Mn-containing intermediates and computational calculations

Since the catalytic reactions were performed in the presence of a base (KOH), it is reasonable to assume that the precatalyst **1** would undergo deprotonation in the presence of KOH to produce **2**, which would serve as the active catalyst. Guided by the recent literature examples of Mn-oxo intermediates that resulted in from Mn(I) and Mn(II) complexes on exposure to light and oxygen,[83,97] we subjected **2** under oxygenated conditions in the presence of blue light and monitored the reaction progress by UV–visible spectroscopy (Figure 5).

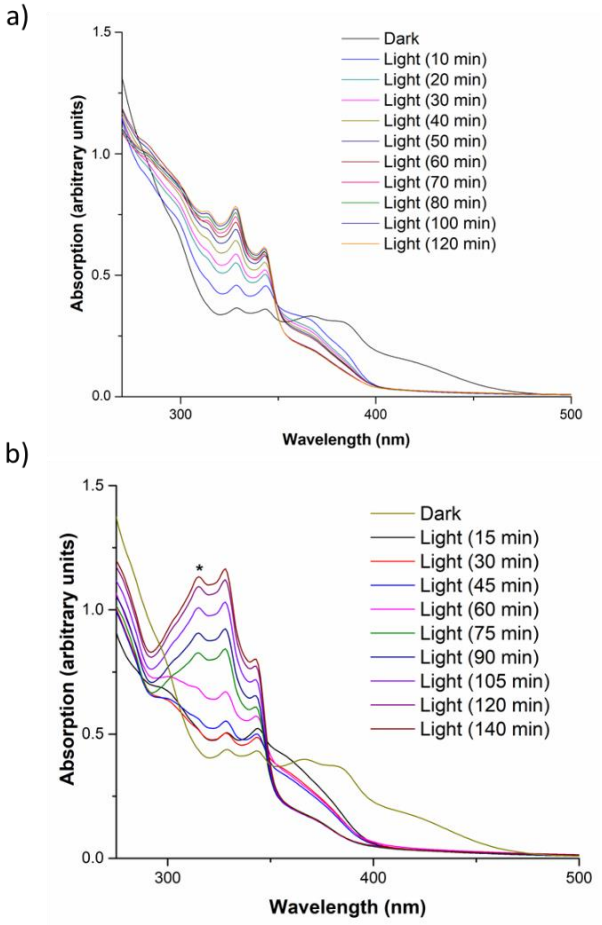

Figure 5. UV-visible spectra of **2** (starting conc. = 0.18 mM) upon irradiation with blue light in a) deoxygenated DCM and b) oxygenated DCM (* indicates a new absorption band).

At first, the UV-visible spectrum of **2** was recorded in deoxygenated dichloromethane (DCM) under a N_2 atmosphere in the dark (Figure 5a). Then, the same solution was irradiated with blue light under N_2, and the subsequent UV-visible spectra were recorded at various time intervals. To aid the assignment of the optical absorption bands, we performed geometry optimizations by DFT calculations and TD-DFT calculations to predict the nature of the transitions (Figure 6). In the dark, we observed two absorption bands at 328 and 342 nm, possibly due to a mixture of metal to ligand charge transfer (MLCT, Mn → L^1) and π-π* transitions centered on the $\mathbf{L^1}$ of **2** with a small contribution from metal-centered (Mn d → d) transitions. In addition, absorption bands at 383 and 420 nm were observed, which may be attributed to a mixture of metal to ligand charge transfer (MLCT, Mn → $\mathbf{L^1}$, Mn → CO), ligand-to-ligand charge transfer (LL′CT, $\mathbf{L^1}$ → CO), with minor contributions of LMCT ($\mathbf{L^1}$ → Mn) based on the TD-DFT calculations. Subsequently, we repeated the aforementioned experiments using oxygenated DCM as the solvent, and the respective UV-visible spectra were recorded at various time intervals (Figure 5b).

We observed that the visible absorption bands disappeared after 15 min of irradiation. After 2 h, a new absorption band at 315 nm appeared prominently (* in Figure 5b), and the bands at 328 and 342 nm increased in intensity. These observations are indicative of the formation of new oxidized Mn intermediates.[100]

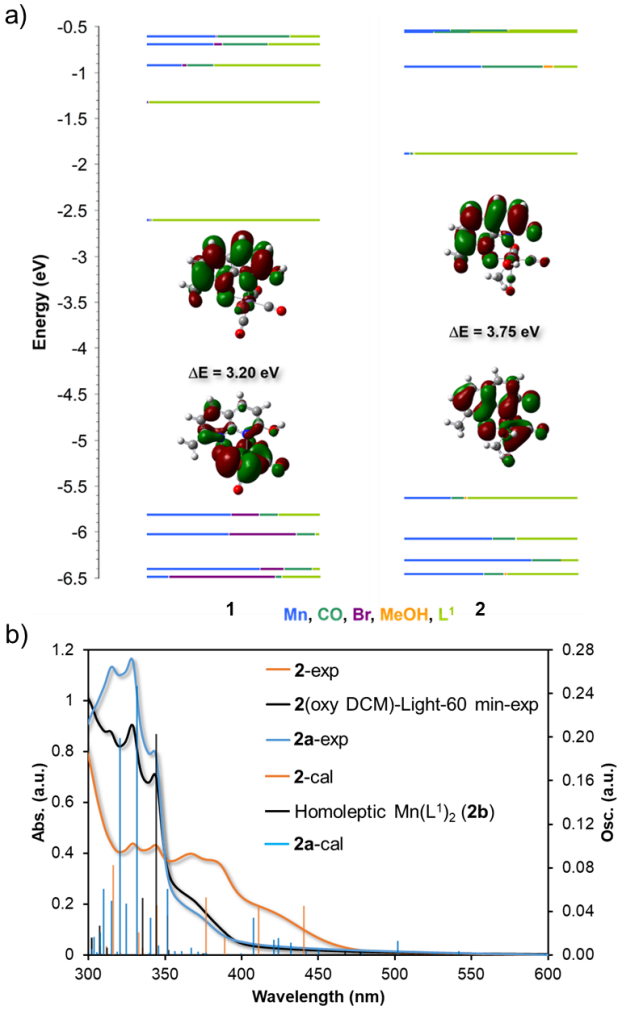

Figure 6. a) The DFT-calculated MOs of **1** and **2** and the HOMO-LUMO energy gap. b) The TD-DFT predicted transitions in **2**, a hypothetical homoleptic Mn($\mathbf{L^1}$)$_2$ (**2b**), and the proposed active catalyst **2a**. The abbreviations used in the spectrum are the following, experimental: exp, oxygenated: oxy, and calculated: cal.

Since there was a dramatic loss of the visible absorption bands within the first 15 min, we proceeded to monitor a solution of **2** in air by FT-IR and NMR spectroscopy as well. The IR spectrum of **2** in the dark shows vibrational bands at 1896 and 2028 cm^{-1}, which can be attributed to the Mn-bound terminal CO (Figure 7a). A carbonyl stretch of $\mathbf{L^1}$ is observed at 1625 cm^{-1}, suggesting that it binds in the lactam form in **2**.[90] On irradiation with blue light, the intensity of the Mn-bound CO bands (1896 and 2028 cm^{-1}) decreased, whereas the carbonyl stretch of $\mathbf{L^1}$ at 1625 cm^{-1} only diminished slightly (Figure 7a), supporting our hypothesis that the activation of **2** starts with photolysis of the CO ligands. Moreover, the ^{1}H NMR spectra recorded during the first 15 min after exposure to blue light under aerobic conditions showed a broadening and decrease in the peak intensities of $\mathbf{L^1}$, consistent with the formation of a paramagnetic higher valent Mn species (see Supporting Information, Figure S2). The dissociation of CO localizes the electron density on $\mathbf{L^1}$ and increases the transition dipole moment of the π-π* absorption, which, in turn, increases the intensity of the bands at 328 and 342 nm. The DFT and TD-DFT calculations conducted on a hypothetical carbonyl-free mononuclear homoleptic $Mn(\mathbf{L^1})_2$ complex (**2b**) and a binuclear $Mn_2(\mathbf{L^1})_2$ complex were consistent with our hypothesis (Figure 6b).

In a separate experiment, the solution of **2** in oxygenated DCM was irradiated with blue light for 15 min, which was then stirred for 2 h in the dark under aerobic conditions. Although the MLCT bands at 383 and 420 nm are reduced in intensity (after first 15 min), no significant changes were observed in the UV-visible spectra in the dark conditions (Figure S3). Particularly, the new peak at 315 nm did not appear after 2 h of stirring in dark under aerobic conditions (c.f. Figure 5b).

In order to characterize the catalytic intermediate that formed after photoinitiation, we isolated the compound after treating **2** in oxygenated DCM with exposure to blue light over a period of 2 h (See Experimental Section). The UV-visible spectrum of the isolated compound (**2a**, see Scheme 6 and Figure 7b) shows similar spectral features at 315, 328, and 342 nm that were observed previously after 2 h exposure of **2** to blue light in oxygenated DCM (c.f. Figure 5b). In the IR spectrum of **2a** (Figure 7c), we did not observe any bands between 1800 – 2200 cm^{-1} that would have originated from CO ligands coordinated to Mn. Nonetheless, we detected stretching bands at 1264 and 1626 cm^{-1}, which can be assigned to the *N*-oxide and carbonyl bands of $\mathbf{L^1}$, respectively (Figure 7c). These data suggest the formation of a higher valent Mn intermediate with no bound CO ligands.[101] We also conducted ESI-MS experiments on **2a**, and found that it exhibits a signal at *m/z* of 529.9899 (see Supporting Information, Figures S4 and S5), which is consistent with $[\mathbf{2a} + Na]^+$.

In addition, when we recorded the ESI-MS of **2** in oxygenated DCM after exposure to blue light for 2 h, a peak at 507.9899 was observed, which corresponds to $[\mathbf{2a}+H]^+$ (see Supporting Information, Figure S6 and S7). Moreover, the ESI-MS (Supporting Information, Figure S6) also exhibited a signal at *m/z* of 668.0358, which may have the structure of **2c** (see, Supporting Information, Figure S8). It probably consists of a binuclear oxidized Mn intermediate containing methoxy bridges supported by the deprotonated $\mathbf{L^1}$. The acetonitrile molecules bound to the Mn probably arose from the solvent used for the ESI-MS measurement.

Scheme 6. Conversion of 2 in oxygenated DCM on irradiation with blue light after 4 h, as detected by ESI-MS.

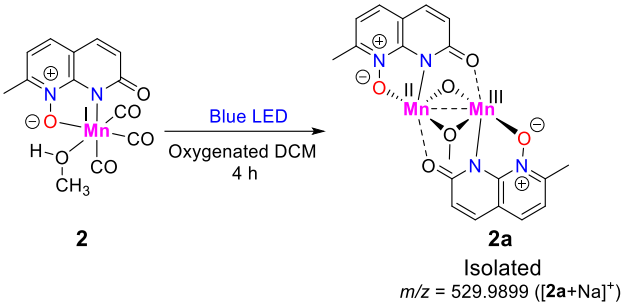

The structure of **2a** was further optimized at the B3LYP-D3BJ level and TD-DFT calculations were conducted using the optimized structure with DCM solvation at the CPCM level. Intense transitions were observed around 313 – 315 nm (Figure 6b), which contain a mixture of the π-π* transition of $\mathbf{L^1}$ and LMCT from the μ-oxo bridge and $\mathbf{L^1}$ to Mn^{III}. The appearance of a minor band at 315 nm in the deoxygenated DCM solution (Figure 5a) may be due to inadvertent O_2 leaks into our cuvette during prolonged irradiation (*vide supra*).

X-ray photoelectron spectroscopy (XPS) was then used to examine the surface elemental properties (Figure S11), including the oxidation states of Mn in **2a**. The high resolution XPS data of the C 1s (Figure S11b) and O 1s (Figure S11d) regions show the respective peaks located at 284.6 and 530.4 eV, the former of which was used to calibrate the spectra.[102] Interestingly, for the N 1s region, two distinct peaks located at 398.5 and 401.5 eV can be observed (Figure S11c), corresponding to the pyridine N and the quaternary N of the N-oxide respectively, which also supports the proposed structure of **2a**.[102] The high resolution Mn 2p XPS of **2a** (Figure 7d) shows the two expected spin-orbit splitting into the $2p_{1/2}$ and $2p_{3/2}$ components. Both the Mn $2p_{1/2}$ and $2p_{3/2}$ peaks were fit and revealed the presence of three Mn oxidation states. The binding energies at 640.5 and 641.8 eV are consistent with the Mn(II) and Mn(III) $2p_{3/2}$ signals,[103,104] while the binding energies at 652.2 and 653.6 eV are consistent with the Mn(II) and Mn(III) $2p_{1/2}$ regions, respectively.[103] We also observed the presence of small amounts of Mn(IV) at 656.8 eV for $2p_{1/2}$ and 644.8 eV for $2p_{3/2}$.[103-105]

Quantitative analysis suggests that the relative elemental composition is 45.4% Mn(III), 31.9% Mn(II), and 22.7% Mn(IV), while energy gap between $2p_{3/2}$ and $2p_{1/2}$ is in the range of 11.7-12 eV, which are within the expected range for a reasonable fit.[105] Thus, the XPS analysis of **2a** supports the presence of oxidized predominantly Mn(III) in the sample, in line with our proposed Mn(III) μ-oxo structure based on the other spectroscopic techniques and DFT calculations, although we cannot conclude the nuclearity of **2a**. Unfortunately, multiple attempts to crystallize the isolated Mn intermediate(s) have been unsuccessful so far.

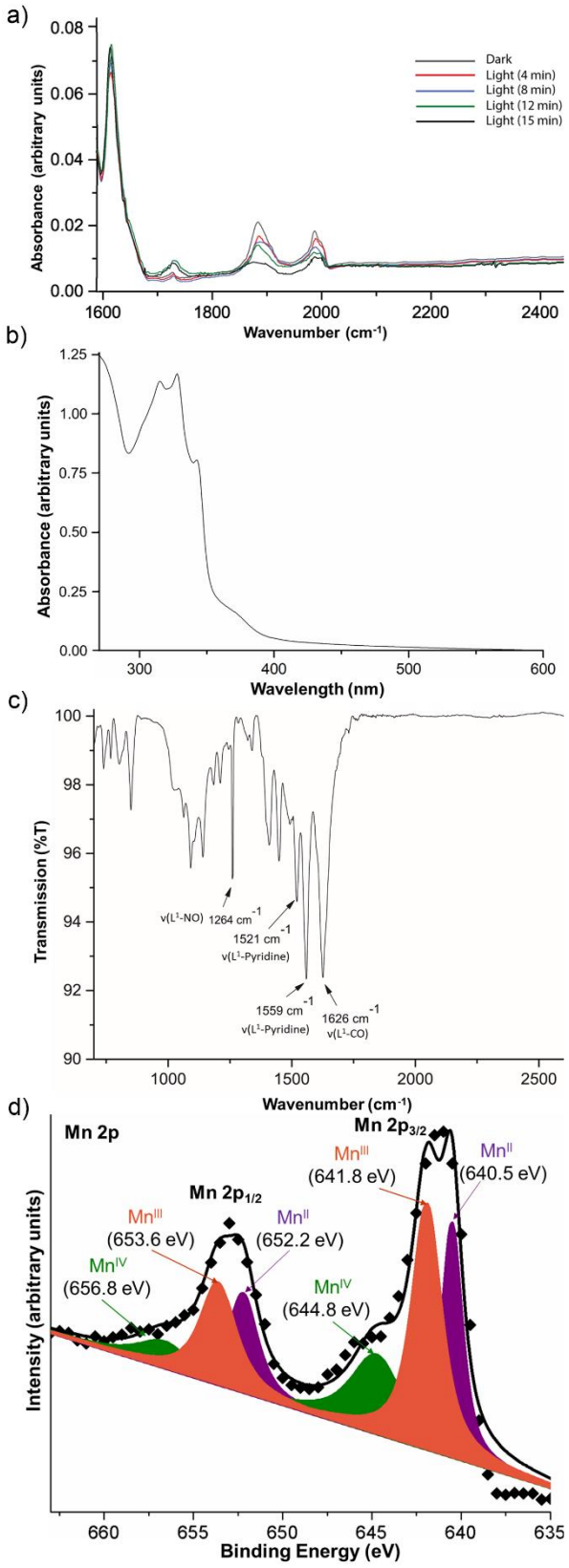

Figure 7. a) FT-IR spectra of **2** under oxygenated conditions during 15 min of blue light irradiation. b) UV-visible spectrum of **2a** in DCM. c) FT-IR spectrum of **2a**. d) XPS data of Mn 2p of **2a**.

To decipher whether the catalytic reaction required prolonged irradiation or whether it was photoinitiated, we performed the reaction between **3a** and acetophenone under the optimized conditions but with only 2 h of illumination, followed by stirring in the dark for 46 h (Scheme 7a). A 75% yield of **4a** was observed by GC-MS spectrometry. We then repeated the same experiment, but with only 15 min of blue light irradiation, followed by 48 h of stirring in the dark, but we observed only a 10% yield of **4a** (Scheme 7b). We also employed **2a** as the catalyst in the dark under otherwise identical conditions as above, which led to a 70% yield of **4a** (Scheme 7c). These experiments suggest that under the reaction conditions, a minimum duration of over 2 h of photoinitiation is required, during which the active Mn catalytic intermediate is formed (*vide supra*).

Scheme 7. Experiments to understand the role of light in the Mn-photocatalyzed reactions. a) Photoinitiation for only 2 h. b) Photoinitiation for only 15 min. c) Dark reaction using the isolated 2a.

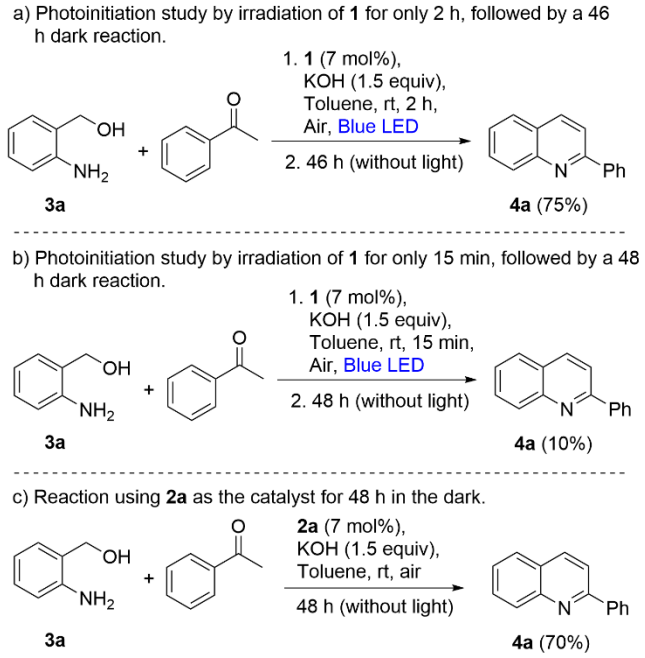

Furthermore, the evolution of **2** under oxygenated conditions in the presence of blue light was investigated using electron paramagnetic resonance (EPR) spectroscopy. The EPR spectra of **2** in deoxygenated DCM both in the light and in the dark suggested that **2** is EPR silent, consistent with its identity as a diamagnetic d^6 low-spin complex. The EPR experiments were then conducted in oxygenated DCM, and as expected, the solution of **2** in the dark was again EPR silent. However, after being exposed to blue light for 2 h, the EPR spectrum showed a low-intensity broad signal at g = ~ 2.03, along with another broad signal at g = ~ 4.78 (Figure 8a).

Notably, an EPR spectrum resembling closely to the spectrum of **2** at low-field in the presence of oxygen and light has previously been reported for ferro- or antiferromagnetically coupled Mn(II)Mn(III) systems with bridging alkoxide ligands.[101] To better understand the nature of these oxidized intermediates during the catalytic cycle, we added methanol to the same solution of **2** in oxygenated DCM from which the EPR spectrum was collected earlier. Interestingly, we observed an increase in

the solubility of the complex and a transformation of the spectrum to one containing the distinctive sextet hyperfine splitting consistent with a g = ~ 2.03 of a Mn(II) species (Figure 8b).

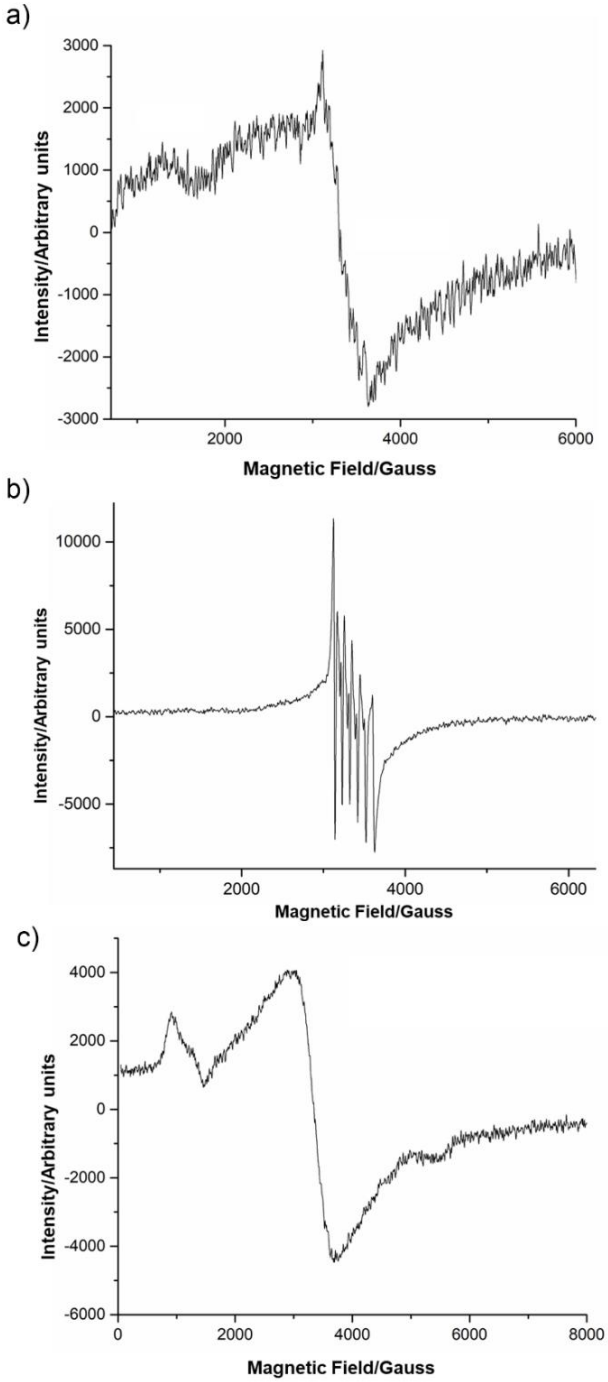

Figure 8. EPR spectra of **2** (29 mM) at 120 K upon irradiation with blue light in a) oxygenated DCM, and b) oxygenated DCM/methanol. c) EPR spectrum of **2a** (isolated solid) at 130 K.

This observation suggests that the high-valent Mn intermediate(s) that formed in oxygenated DCM was likely to have reacted with methanol to convert into a more stable, but probably catalytically inactive Mn(II) resting intermediate. We isolated the material after introduction to methanol and indeed found that the yield of **4a** was negligible in the absence of light under the otherwise optimized conditions. We then tried to independently synthesize the intermediates by treating **2** with 3 equivalents of PhIO, but observed different species, likely arising from over-oxidized Mn products (Supporting Information, Figure S10). On the other hand, an EPR spectrum of **2a** in the solid-state showed a low-intensity broad signal at g = ~ 2.02, along with another broad signal at g = ~ 5.68 (Figure 8c), which closely resembles the catalytically active intermediate that we observed after 2 h of irradiation (Figure 8a).Overall, the EPR studies confirm the necessity of both blue light and O_2 to convert the Mn(I) pre-catalyst to oxidized Mn intermediates during the catalytic cycle. Based on the recent work on the photo-driven oxidative cleavage of alkenes by non-heme Mn catalysts in the presence of O_2,[97] and our experimental observations, we hypothesize that the Mn(II) resting state will further react with O_2 during the catalytic cycle to generate higher valent Mn μ-oxo intermediates (see, ESI-MS discussion below) that oxidize the benzyl alcohol substrates. The electrophilic Mn-oxo intermediates are known to follow a $2e^-$ oxidative pathway from benzyl alcohol to benzaldehyde by the activation of benzylic-CH bonds.[106]

CONCLUSION

A Mn(I) complex featuring a hydroxy-functionalized naphthyridine *N*-oxide ligand was employed for the photocatalytic aerobic synthesis of quinolines from 2-aminobenzyl alcohols and ketones in the presence of visible light. The scope of the substrate included a wide range of electronic properties. We observed that the yields of the products appeared to be lower for the ketones with electron-rich substituents on the aromatic ring, as well as the aliphatic ketones. This can be rationalized by the fact that the decreased electrophilicity of the carbonyl group of the ketone may lead to less favorable formation of **I-1** (Step-1, Scheme 4). On the other hand, electron-donating functional groups on the 2-aminobenzyl alcohols generally provided higher yields of the corresponding products, which may be because the increased nucleophilicity of the amine favored the formation of **I-1** (Step-1), and also facilitated the Mn-catalyzed oxidation to form **I-2** (Step-2, Scheme 4). Moreover, the catalytic protocol was also efficient for the functionalization of bioactive steroids and the synthesis of a derivative of the antimalarial drug chloroquine. Substrate viability experiments, UV-visible, EPR, and XPS studies suggest a three-step reaction pathway involving a visible light driven oxidative Mn photocatalytic reaction. Further utilization of this Mn photocatalyst in challenging acceptorless dehydrogenation reactions is currently being investigated in our laboratory.

EXPERIMENTAL SECTION

General Experimental Details. The reactions with the Mn complexes were carried out under an atmosphere of purified nitrogen using standard Schlenk– and vacuum-line techniques. The ^{1}H NMR spectra were obtained on JEOL JNM–LA 500MHz and JEOL JNM–LA 400MHz spectrometers. The ^{1}H NMR chemical shifts were referenced to the residual hydrogen signal of the deuterated solvents. The chemical shift is given as dimensionless δ values and is referenced relative to TMS for

both ^{1}H and ^{13}C NMR spectroscopy. GC–MS experiments were performed on an Agilent 7890A GC and 5975C MS system. The ESI–MS were recorded on a Waters Micromass Quattro Micro triple-quadrupole mass spectrometer. UV–visible spectra were recorded using a JASCO V–670 UV-visible absorption spectrophotometer. EPR measurements were performed on a Bruker Biospin GmbH instrument.

Materials. The solvents were purified by conventional methods, distilled under N_2, and deoxygenated prior to use. $Mn(CO)_5Br$, 2,6-diaminopyridine, substrates **3a-e**, 2-trifluoromethyl-5-bromopyridine, chlorodiphenylphosphine, DBU, *n*-BuLi, 2-amino-5-diethylaminopentane, $Pd(OAc)_2$, and DPEphos were purchased from Sigma-Aldrich. All ketones and Tf_2O were purchased from TCI chemicals.

UV–Visible Monitoring: The stock solutions of **2** (1.0 mM) were prepared in anhydrous DCM (both oxygenated and deoxygenated). In each experiment, 400 μL of the stock solution of **2** was pipetted into a quartz cuvette and diluted to 2.2 mL. When deoxygenated DCM was used to provide a completely O_2-free environment, the solution of **2** was prepared inside a glovebox and sealed before taking it out to perform the experiments in the dark and in the presence of blue light. When oxygenated DCM was used, the solution of **2** was prepared under an ambient aerobic environment. Further experiments were then conducted in air.

EPR Experiments: The solutions of **2** (20 mg in 2 mL of solvent) were prepared in anhydrous DCM (both oxygenated and deoxygenated). In each experiment, 200 μL of the stock solution was pipetted into a 4 mm outer diameter/3 mm inner diameter Suprasil quartz EPR tube (Wilmad LabGlass) and frozen in liquid N_2. We have followed a similar procedure as discussed in the UV-visible spectroscopy experiments to prepare the solutions in a completely O_2-free environment in deoxygenated DCM or in oxygenated DCM under an ambient aerobic environment. Another EPR spectrum was recorded by adding 50 μL of methanol to the blue-light exposed (2 h) oxygenated DCM solution of **2**.

ESI-MS Experiments: The solution of **2** (10 mg in 2 mL of solvent) was prepared in oxygenated anhydrous DCM. After 2 h of exposure to blue light, 500 μL of the stock solution was pipetted out and 50 μL of acetonitrile was added. This solution was then injected into the ESI-MS.

XPS Experiment: X-ray photoelectron spectroscopy (XPS) was performed using a Kratos AXIS Supra spectrometer with a monochromatic Al K_α source (15 mA, 15 kV). A 3.1 V bias was applied to the sample to neutralize the positive charge buildup on the sample surface. Individual core levels were measured with a pass energy of 20 eV. XPS measurements were performed on a solid powder sample pressed onto SPI double-sided adhesive carbon tape. The XPS data obtained were processed using the ESCApe software (Kratos Analytical). The spectra were calibrated internally by setting the C 1s signal to 284.6 eV.

General Procedure for the Synthesis of Quinoline Derivatives Using 2-Aminobenzyl Alcohols and Ketones: A mixture of **1** (0.0070 mmol), a 2-aminobenzyl alcohol (1.00 equivalent, 0.100 mmol), a ketone (1.00 equivalent, 0.100 mmol), and KOH (1.50 equivalent, 0.150 mmol) in 3 mL of toluene were placed in a Schlenk tube. The reaction mixture was stirred at room temperature with irradiation using a 50 W blue LED for 48-72 h under air. Subsequently, the solvent was removed *in vacuo*. The residue was purified by column chromatography on silica gel using hexane/EtOAc as the eluent and the corresponding isolated yields are obtained as reported in the figures of the discussion.

Procedure for the Isolation of 2a: Complex **2** was dissolved in oxygenated anhydrous DCM and the solution was stirred under blue light irradiation for 4 h. Then, the DCM was removed in vacuo, which resulted in a brown residue. The residue was further washed with anhydrous hexane (3 x 10 mL) and dried under vacuum.

AUTHOR INFORMATION

Corresponding Authors

Prof. Han Sen Soo − School of Chemistry, Chemical Engineering and Biotechnology, Nanyang Technological University, Singapore, 21 Nanyang Link, Singapore 637371. E-mail: hansen@ntu.edu.sg

Prof. Jitendra K. Bera − Department of Chemistry and Centre for Environmental Science and Engineering, Indian Institute of Technology Kanpur, Kanpur 208016, India; orcid.org/0000-0002-5689-8863; Email: jbera@iitk.ac.in

Authors:

Kamaless Patra − Department of Chemistry and Centre for Environmental Science and Engineering, Indian Institute of Technology Kanpur, Kanpur 208016, India

Arindom Bhattacherya − Department of Chemistry and Centre for Environmental Science and Engineering, Indian Institute of Technology Kanpur, Kanpur 208016, India

Chenfei Li − School of Chemistry, Chemical Engineering and Biotechnology, Nanyang Technological University, Singapore, 21 Nanyang Link, Singapore 637371.

Author Contributions

[†‡]K.P and [†]A.B contributed equally to this work.

Notes

The authors declare no competing financial interest.

Supporting Information

The Supporting Information is available free of charge on the ACS Publications website.

Experimental details for the syntheses and condition optimization. NMR, UV-visible, EPR, XPS, and ESI-MS spectral data, DFT calculated coordinates, and supporting figures. (PDF)

ACKNOWLEDGMENT

H.S.S. acknowledges that this project is supported by A*STAR under the AME IRG grant no. A2083c0050. H.S.S. is also grateful for the Singapore Ministry of Education Academic Research Fund Tier 1 grants RT 05/19 and RG 09/22, and the NTU 5th ACE Grant Call. Financial support from the Science and Engineering Research Board (SERB), India is gratefully acknowledged. J.K.B. thanks SERB, India, for a J. C. Bose fellowship. K.P. thanks NTU, Singapore and the International Internship Program (IIP) for a fellowship. A.B. thanks IIT Kanpur for fellowship.

REFERENCES

(1) Vitaku, E.; Smith, D. T.; Njardarson, J. T. Analysis of the Structural Diversity, Substitution Patterns, and Frequency of Nitrogen Heterocycles among U.S. FDA Approved Pharmaceuticals. *J. Med. Chem.* **2014**, *57* (24), 10257–10274. https://doi.org/10.1021/jm501100b.

(2) De Los Ríos, C.; Egea, J.; Marco-Contelles, J.; León, R.; Samadi, A.; Iriepa, I.; Moraleda, I.; Gálvez, E.; García, A. G.; López, M. G.; Villarroya, M.; Romero, A. Synthesis, Inhibitory Activity of Cholinesterases, and Neuroprotective Profile of Novel 1,8-Naphthyridine Derivatives. *J. Med. Chem.* **2010**, *53* (14), 5129–5143. https://doi.org/10.1021/jm901902w.

(3) Nakatani, K.; Hagihara, S.; Sando, S.; Sakamoto, S.; Yamaguchi, K.; Maesawa, C.; Saito, I. Induction of a Remarkable Conformational Change in a Human Telomeric Sequence by the Binding of Naphthyridine Dimer: Inhibition of the Elongation of a Telomeric Repeat by Telomerase. *J. Am. Chem. Soc.* **2003**, *125* (3), 662–666. https://doi.org/10.1021/ja027055g.

(4) Sriram, D.; Senthilkumar, P.; Dinakaran, M.; Yogeeswari, P.; China, A.; Nagaraja, V. Antimycobacterial Activities of Novel 1-(Cyclopropyl/Tert-Butyl/4- Fluorophenyl)-1,4-Dihydro-6-Nitro-4-Oxo-7-(Substituted Secondary Amino)-1,8-Naphthyridine-3-Carboxylic Acid. *J. Med. Chem.* **2007**, *50* (24), 6232–6239. https://doi.org/10.1021/jm700999n.

(5) Nam, T. G.; Rector, C. L.; Kim, H. Y.; Sonnen, A. F. P.; Meyer, R.; Nau, W. M.; Atkinson, J.; Rintoul, J.; Pratt, D. A.; Porter, N. A. Tetrahydro-1,8-Naphthyridinol Analogues of α-Tocopherol as Antioxidants in Lipid Membranes and Low-Density Lipoproteins. *J. Am. Chem. Soc.* **2007**, *129* (33), 10211–10219. https://doi.org/10.1021/ja072371m.

(6) Motati, D. R.; Uredi, D.; Watkins, E. B. A General Method for the Metal-Free, Regioselective, Remote C-H Halogenation of 8-Substituted Quinolines. *Chem. Sci.* **2018**, *9* (7), 1782–1788. https://doi.org/10.1039/c7sc04107a.

(7) Wendlandt, A. E.; Stahl, S. S. Modular O-Quinone Catalyst System for Dehydrogenation of Tetrahydroquinolines under Ambient Conditions. *J. Am. Chem. Soc.* **2014**, *136* (34), 11910–11913. https://doi.org/10.1021/ja506546w.

(8) Dong, J.; Lyu, X.; Wang, Z.; Wang, X.; Song, H.; Liu, Y.; Wang, Q. Visible-Light-Mediated Minisci C-H Alkylation of Heteroarenes with Unactivated Alkyl Halides Using O2 as an Oxidant. *Chem. Sci.* **2019**, *10* (4), 976–982. https://doi.org/10.1039/c8sc04892d.

(9) Lai, X.-L.; Shu, X.-M.; Song, J.; Xu, H.-C. Electrophotocatalytic Decarboxylative C−H Functionalization of Heteroarenes. *Angew. Chem. Int. Ed.* **2020**, *59* (26), 10626–10632. https://doi.org/10.1002/anie.202002900.

(10) Jin, J.; MacMillan, D. W. C. Alcohols as Alkylating Agents in Heteroarene C-H Functionalization. *Nature* **2015**, *525* (7567), 87–90. https://doi.org/10.1038/nature14885.

(11) Pony Yu, R.; Hesk, D.; Rivera, N.; Pelczer, I.; Chirik, P. J. Iron-Catalysed Tritiation of Pharmaceuticals. *Nature* **2016**, *529* (7585), 195–199. https://doi.org/10.1038/nature16464.

(12) Gorka, A. P.; De Dios, A.; Roepe, P. D. Quinoline Drug-Heme Interactions and Implications for Antimalarial Cytostatic versus Cytocidal Activities. *J. Med. Chem.* **2013**, *56* (13), 5231–5246. https://doi.org/10.1021/jm400282d.

(13) Ridley, R. G. Medical Need, Scientific Opportunity and the Drive for Antimalarial Drugs. *Nature* **2002**, *415* (6872), 686–693. https://doi.org/10.1038/415686a.

(14) Marco-Contelles, J.; Pérez-Mayoral, E.; Abdelouahid Samadi; Carreiras, M. D. C.; Soriano, E. Recent Advances in the Friedländer Reaction. *Chem. Rev.* **2009**, *109* (6), 2652–2671. https://doi.org/10.1021/cr800482c.

(15) Bañón-Caballero, A.; Guillena, G.; Nájera, C. Solvent-Free Enantioselective Friedländer Condensation with Wet 1,1′-Binaphthalene-2,2′-Diamine-Derived Prolinamides as Organocatalysts. *J. Org. Chem.* **2013**, *78* (11), 5349–5356. https://doi.org/10.1021/jo400522m.

(16) Anderson, E. C.; Sneddon, H. F.; Hayes, C. J. A Mild Synthesis of Substituted 1,8-Naphthyridines. *Green Chem.* **2019**, *21* (11), 3050–3058. https://doi.org/10.1039/c9gc00408d.

(17) Tanwar, B.; Kumar, D.; Kumar, A.; Ansari, M. I.; Qadri, M. M.; Vaja, M. D.; Singh, M.; Chakraborti, A. K. Friedländer Annulation: Scope and Limitations of Metal Salt Lewis Acid Catalysts in Selectivity Control for the Synthesis of Functionalised Quinolines. *New J. Chem.* **2015**, *39* (12), 9824–9833. https://doi.org/10.1039/c5nj02010g.

(18) Jiang, B.; Dong, J. J.; Jin, Y.; Du, X. L.; Xu, M. The First Proline-Catalyzed Friedlander Annulation: Regioselective Synthesis of 2-Substituted Quinoline Derivatives. *Eur. J. Org. Chem.* **2008**, *2008* (16), 2693–2696. https://doi.org/10.1002/ejoc.200800121.

(19) Wu, J.; Xia, H. G.; Gao, K. Molecular Iodine: A Highly Efficient Catalyst in the Synthesis of Quinolines via Friedländer Annulation. *Org. Biomol. Chem.* **2006**, *4* (1), 126–129. https://doi.org/10.1039/b514635f.

(20) Chakraborty, G.; Sikari, R.; Das, S.; Mondal, R.; Sinha, S.; Banerjee, S.; Paul, N. D. Dehydrogenative Synthesis of Quinolines, 2-Aminoquinolines, and Quinazolines Using Singlet Diradical Ni(II)-Catalysts. *J. Org. Chem.* **2019**, *84* (5), 2626–2641. https://doi.org/10.1021/acs.joc.8b03070.

(21) Maji, M.; Chakrabarti, K.; Panja, D.; Kundu, S. Sustainable Synthesis of N-Heterocycles in Water Using Alcohols Following the Double Dehydrogenation Strategy. *J. Catal.* **2019**, *373*, 93–102. https://doi.org/10.1016/j.jcat.2019.03.028.

(22) Elangovan, S.; Sortais, J. B.; Beller, M.; Darcel, C. Iron-Catalyzed α-Alkylation of Ketones with Alcohols. *Angew. Chem. Int. Ed.* **2015**, *54* (48), 14483–14486. https://doi.org/10.1002/anie.201506698.

(23) Pavithra, D.; Ethiraj, K. R.; Nawaz Khan, F. R. Cu-TEMPO Catalyzed Dehydrogenative Friedlander Annulation/Sp3 C–H Functionalization/Spiroannulation towards Spiro[Indoline-3,3'-Pyrrolizin]-2'-Yl)-4-Phenylquinoline-3-Carboxylates. *Eur. J. Org. Chem.* **2020**, *2020* (45), 7035–7050. https://doi.org/10.1002/ejoc.202001109.

(24) Das, S.; Maiti, D.; De Sarkar, S. Synthesis of Polysubstituted Quinolines from α-2-Aminoaryl Alcohols Via Nickel-Catalyzed Dehydrogenative Coupling. *J. Org. Chem.* **2018**, *83* (4), 2309–2316. https://doi.org/10.1021/acs.joc.7b03198.

(25) Mastalir, M.; Glatz, M.; Pittenauer, E.; Allmaier, G.; Kirchner, K. Sustainable Synthesis of Quinolines and Pyrimidines Catalyzed by Manganese PNP Pincer Complexes. *J. Am. Chem. Soc.* **2016**, *138* (48), 15543–15546. https://doi.org/10.1021/jacs.6b10433.

(26) Singh, K.; Vellakkaran, M.; Banerjee, D. A Nitrogen-Ligated Nickel-Catalyst Enables Selective Intermolecular Cyclisation of β- And γ-Amino Alcohols with Ketones: Access to Five and Six-Membered N-Heterocycles. *Green Chem.* **2018**, *20* (10), 2250–2256. https://doi.org/10.1039/c8gc00318a.

(27) Lan, X. B.; Ye, Z.; Huang, M.; Liu, J.; Liu, Y.; Ke, Z. Nonbifunctional Outer-Sphere Strategy Achieved Highly Active α-Alkylation of Ketones with Alcohols by N-Heterocyclic Carbene Manganese (NHC-Mn). *Org. Lett.* **2019**, *21* (19), 8065–8070. https://doi.org/10.1021/acs.orglett.9b03030.

(28) Pan, B.; Liu, B.; Yue, E.; Liu, Q.; Yang, X.; Wang, Z.; Sun, W. H. A Ruthenium Catalyst with Unprecedented Effectiveness for the Coupling Cyclization of - Amino Alcohols and Secondary Alcohols. *ACS Catal.* **2016**, *6* (2), 1247–1253. https://doi.org/10.1021/acscatal.5b02638.

(29) Parua, S.; Sikari, R.; Sinha, S.; Das, S.; Chakraborty, G.; Paul, N. D. A Nickel Catalyzed Acceptorless Dehydrogenative Approach to Quinolines. *Org. Biomol. Chem.* **2018**, *16* (2), 274–284. https://doi.org/10.1039/c7ob02670f.

(30) Das, K.; Mondal, A.; Pal, D.; Srimani, D. Sustainable Synthesis of Quinazoline and 2-Aminoquinoline via Dehydrogenative Coupling of 2-Aminobenzyl Alcohol and Nitrile Catalyzed by Phosphine-Free Manganese Pincer Complex. *Org. Lett.* **2019**, *21* (9), 3223–3227. https://doi.org/10.1021/acs.orglett.9b00939.

(31) Wang, R.; Fan, H.; Zhao, W.; Li, F. Acceptorless Dehydrogenative Cyclization of O-Aminobenzyl Alcohols with Ketones to Quinolines in Water Catalyzed by Water-Soluble Metal-Ligand Bifunctional Catalyst [Cp∗(6,6′-(OH)2bpy)(H2O)][OTf]2. *Org. Lett.* **2016**, *18* (15), 3558–3561. https://doi.org/10.1021/acs.orglett.6b01518.

(32) Wei, D.; Dorcet, V.; Darcel, C.; Sortais, J. B. Synthesis of Quinolines Through Acceptorless Dehydrogenative Coupling Catalyzed by Rhenium PN(H)P Complexes. *ChemSusChem* **2019**, *12* (13), 3078–3082. https://doi.org/10.1002/cssc.201802636.

(33) Daw, P.; Kumar, A.; Espinosa-Jalapa, N. A.; Diskin-Posner, Y.; Ben-David, Y.; Milstein, D. Synthesis of Pyrazines and Quinoxalines via Acceptorless Dehydrogenative Coupling Routes Catalyzed by Manganese Pincer Complexes. *ACS Catal.* **2018**, *8* (9), 7734–7741. https://doi.org/10.1021/acscatal.8b02208.

(34) Srimani, D.; Ben-David, Y.; Milstein, D. Direct Synthesis of Pyridines and Quinolines by Coupling of γ-Amino-Alcohols with Secondary Alcohols Liberating H2 Catalyzed by Ruthenium Pincer Complexes. *Chem. Commun.* **2013**, *49* (59), 6632–6634. https://doi.org/10.1039/c3cc43227k.

(35) Mondal, R.; Herbert, D. E. Synthesis of Pyridines, Quinolines, and Pyrimidines via Acceptorless Dehydrogenative Coupling Catalyzed by a Simple Bidentate P^ N Ligand Supported Ru Complex. *Organometallics* **2020**, *39* (8), 1310–1317. https://doi.org/10.1021/acs.organomet.0c00058.

(36) Chaudhari, C.; Sato, K.; Ogura, Y.; Miayahara, S. I.; Nagaoka, K. Pr2O3 Supported Nano-Layered Ruthenium Catalyzed Acceptorless Dehydrogenative Synthesis of 2-Substituted Quinolines and 1,8-Naphthyridines from 2-Aminoaryl Alcohols and Ketones. *ChemCatChem* **2020**, *12* (8), 2198–2202. https://doi.org/10.1002/cctc.201902311.

(37) Vander Mierde, H.; Ledoux, N.; Allaert, B.; Vander Voort, P.; Drozdzak, R.; De Vos, D.; Verpoort, F. Improved Ruthenium Catalysts for the Modified Friedlaender Quinoline Synthesis. *New J. Chem.* **2007**, *31* (9), 1572−1574. https://doi.org/10.1039/B707292A.

(38) Anand, N.; Koley, S.; Ramulu, B. J.; Singh, M. S. Metal-Free Aerobic One-Pot Synthesis of Substituted/Annulated Quinolines from Alcohols via Indirect Friedländer Annulation. *Org. Biomol. Chem.* **2015**, *13* (37), 9570–9574. https://doi.org/10.1039/c5ob01422k.

(39) Yan, R.; Liu, X.; Pan, C.; Zhou, X.; Li, X.; Kang, X.; Huang, G. Aerobic Synthesis of Substituted Quinoline from Aldehyde and Aniline: Copper-Catalyzed Intermolecular C-H Active and C-C Formative Cyclization. *Org. Lett.* **2013**, *15* (18), 4876–4879. https://doi.org/10.1021/ol402312h.

(40) Bains, A. K.; Singh, V.; Adhikari, D. Homogeneous Nickel-Catalyzed Sustainable Synthesis of Quinoline and Quinoxaline under Aerobic Conditions. *J. Org. Chem.* **2020**, *85* (23), 14971–14979. https://doi.org/10.1021/acs.joc.0c01819.

(41) Flanagan, J. C. A.; Dornan, L. M.; McLaughlin, M. G.; McCreanor, N. G.; Cook, M. J.; Muldoon, M. J. The Synthesis of N-Heterocycles via Copper/TEMPO Catalysed Aerobic Oxidation of Amino Alcohols. *Green Chem.* **2012**, *14* (5), 1281–1283. https://doi.org/10.1039/c2gc35062a.

(42) Jayaraj, S.; Badu-Tawiah, A. K. N-Substituted Auxiliaries for Aerobic Dehydrogenation of Tetrahydro-Isoquinoline: A Theory-Guided Photo-Catalytic Design. *Sci. Rep.* **2019**, *9* (1), 11280. https://doi.org/10.1038/s41598-019-47735-y.

(43) Blum, T. R.; Miller, Z. D.; Bates, D. M.; Guzei, I. A.; Yoon, T. P. Enantioselective Photochemistry through Lewis Acid-Catalyzed Triplet Energy Transfer. *Science* **2016**, *354* (6318), 1391–1395. https://doi.org/10.1126/science.aai8228.

(44) Chen, Y.; Du, J.; Zuo, Z. Selective C-C Bond Scission of Ketones via Visible-Light-Mediated Cerium Catalysis. *Chem* **2020**, *6* (1), 266–279. https://doi.org/10.1016/j.chempr.2019.11.009.

(45) Silvi, M.; Melchiorre, P. Enhancing the Potential of Enantioselective Organocatalysis with Light. *Nature* **2018**, *554* (7690), 41–49. https://doi.org/10.1038/nature25175.

(46) Romero, N. A.; Margrey, K. A.; Tay, N. E.; Nicewicz, D. A. Site-Selective Arene C-H Amination via Photoredox Catalysis. *Science* **2015**, *349* (6254), 1326–1330. https://doi.org/10.1126/science.aac9895.

(47) Fukuzumi, S.; Ohkubo, K. Selective Photocatalytic Reactions with Organic Photocatalysts. *Chem. Sci.* **2013**, *4* (2), 561–574. https://doi.org/10.1039/c2sc21449k.

(48) Musacchio, A. J.; Lainhart, B. C.; Zhang, X.; Naguib, S. G.; Sherwood, T. C.; Knowles, R. R. Catalytic Intermolecular Hydroaminations of Unactivated Olefins with Secondary Alkyl Amines. *Science* **2017**, *355* (6326), 727–730. https://doi.org/10.1126/science.aal3010.

(49) Chu, J. C. K.; Rovis, T. Amide-Directed Photoredox-Catalysed C-C Bond Formation at Unactivated Sp 3 C-H Bonds. *Nature* **2016**, *539* (7628), 272–275. https://doi.org/10.1038/nature19810.

(50) Prier, C. K.; Rankic, D. A.; MacMillan, D. W. C. Visible Light Photoredox Catalysis with Transition Metal Complexes: Applications in Organic Synthesis. *Chem. Rev.* **2013**, *113* (7), 5322–5363. https://doi.org/10.1021/cr300503r.

(51) Welin, E. R.; Le, C.; Arias-Rotondo, D. M.; McCusker, J. K.; MacMillan, D. W. C. Photosensitized, Energy Transfer-Mediated Organometallic Catalysis through Electronically Excited Nickel(II). *Science* **2017**, *355* (6323), 380–385. https://doi.org/10.1126/SCIENCE.AAL2490.

(52) Fukuzumi, S.; Ohkubo, K. Organic Synthetic Transformations Using Organic Dyes as Photoredox Catalysts. *Org. Biomol. Chem.* **2014**, *12* (32), 6059–6071. https://doi.org/10.1039/c4ob00843j.

(53) Constantin, T.; Zanini, M.; Regni, A.; Sheikh, N. S.; Juliá, F.; Leonori, D. Aminoalkyl Radicals as Halogen-Atom Transfer Agents for Activation of Alkyl and Aryl Halides. *Science* **2020**, *367* (6481), 1021–1026. https://doi.org/10.1126/science.aba2419.

(54) Gazi, S.; Dokić, M.; Moeljadi, A. M. P.; Ganguly, R.; Hirao, H.; Soo, H. Sen. Kinetics and DFT Studies of Photoredox Carbon-Carbon Bond Cleavage Reactions by Molecular Vanadium Catalysts under Ambient Conditions. *ACS Catal.* **2017**, *7* (7), 4682–4691. https://doi.org/10.1021/acscatal.7b01036.

(55) Gazi, S.; Đokić, M.; Chin, K. F.; Ng, P. R.; Soo, H. Sen. Visible Light–Driven Cascade Carbon–Carbon Bond Scission for Organic Transformations and Plastics Recycling. *Adv. Sci.* **2019**, *6* (24), 1902020. https://doi.org/10.1002/advs.201902020.

(56) Gazi, S.; Hung Ng, W. K.; Ganguly, R.; Putra Moeljadi, A. M.; Hirao, H.; Soo, H. Sen. Selective Photocatalytic C-C Bond Cleavage under Ambient Conditions with Earth Abundant Vanadium Complexes. *Chem. Sci.* **2015**, *6* (12), 7130–7142. https://doi.org/10.1039/c5sc02923f.

(57) Dokić, M.; Soo, H. Sen. Artificial Photosynthesis by Light Absorption, Charge Separation, and Multielectron Catalysis. *Chem. Commun.* **2018**, *54* (50), 6554–6572. https://doi.org/10.1039/c8cc02156b.

(58) Chin, K. F.; Đokić, M.; Soo, H. Sen. Artificial Photosynthesis Beyond Water Splitting for Environmental Remediation. *Trends Chem.* **2020**, *2* (6), 485–488. https://doi.org/10.1016/j.trechm.2020.02.012.

(59) Ru Ng, A. Y.; Boruah, B.; Chin, K. F.; Modak, J. M.; Soo, H. Sen. Photoelectrochemical Cells for Artificial Photosynthesis: Alternatives to Water Oxidation. *ChemNanoMat* **2020**, *6* (2), 185–203. https://doi.org/10.1002/cnma.201900616.

(60) Stevenson, S. M.; Higgins, R. F.; Shores, M. P.; Ferreira, E. M. Chromium Photocatalysis: Accessing Structural Complements to Diels-Alder Adducts with Electron-Deficient Dienophiles. *Chem. Sci.* **2017**, *8* (1), 654–660. https://doi.org/10.1039/c6sc03303b.

(61) Alig, L.; Fritz, M.; Schneider, S. First-Row Transition Metal (De)Hydrogenation Catalysis Based on Functional Pincer Ligands. *Chem. Rev.* **2019**, *119* (4), 2681–2751. https://doi.org/10.1021/acs.chemrev.8b00555.

(62) Higgins, R. F.; Fatur, S. M.; Shepard, S. G.; Stevenson, S. M.; Boston, D. J.; Ferreira, E. M.; Damrauer, N. H.; Rappé, A. K.; Shores, M. P. Uncovering the Roles of Oxygen in Cr(III) Photoredox Catalysis. *J. Am. Chem. Soc.* **2016**, *138* (16), 5451–5464. https://doi.org/10.1021/jacs.6b02723.

(63) Kjær, K. S.; Kaul, N.; Prakash, O.; Chábera, P.; Rosemann, N. W.; Honarfar, A.; Gordivska, O.; Fredin, L. A.; Bergquist, K. E.; Häggström, L.; Ericsson, T.; Lindh, L.; Yartsev, A.; Styring, S.; Huang, P.; Uhlig, J.; Bendix, J.; Strand, D.; Sundström, V.; Persson, P.; Lomoth, R.; Wärnmark, K. Luminescence and Reactivity of a Charge-Transfer Excited Iron Complex with Nanosecond Lifetime. *Science* **2019**, *363* (6424), 249–253. https://doi.org/10.1126/science.aau7160.

(64) Weiss, M. E.; Kreis, L. M.; Lauber, A.; Carreira, E. M. Cobalt-Catalyzed Coupling of Alkyl Iodides with Alkenes: Deprotonation of Hydridocobalt Enables Turnover. *Angew. Chem. Int. Ed.* **2011**, *50* (47), 11125–11128. https://doi.org/10.1002/anie.201105235.

(65) Ociepa, M.; Baka, O.; Narodowiec, J.; Gryko, D. Light-Driven Vitamin B12-Catalysed Generation of Acyl Radicals from 2-S-Pyridyl Thioesters. *Adv. Synth. Catal.* **2017**, *359* (20), 3560–3565. https://doi.org/10.1002/adsc.201700913.

(66) He, K. H.; Tan, F. F.; Zhou, C. Z.; Zhou, G. J.; Yang, X. L.; Li, Y. Acceptorless Dehydrogenation of N-Heterocycles by Merging Visible-Light Photoredox Catalysis and Cobalt Catalysis. *Angew. Chem. Int. Ed.* **2017**, *56* (11), 3080–3084. https://doi.org/10.1002/anie.201612486.

(67) Pal, A. K.; Li, C.; Hanan, G. S.; Zysman-Colman, E. Blue-Emissive Cobalt(III) Complexes and Their Use in the Photocatalytic Trifluoromethylation of Polycyclic Aromatic Hydrocarbons. *Angew. Chem. Int. Ed.* **2018**, *57* (27), 8027–8031. https://doi.org/10.1002/anie.201802532.

(68) Weiss, M. E.; Carreira, E. M. Total Synthesis of (+)-Daphmanidin E. *Angew. Chem. Int. Ed.* **2011**, *50* (48), 11501–11505. https://doi.org/10.1002/anie.201104681.

(69) Kreis, L. M.; Krautwald, S.; Pfeiffer, N.; Martin, R. E.; Carreira, E. M. Photocatalytic Synthesis of Allylic Trifluoromethyl Substituted Styrene Derivatives in Batch and Flow. *Org. Lett.* **2013**, *15* (7), 1634–1637. https://doi.org/10.1021/ol400410m.

(70) Johnson, M. W.; Hannoun, K. I.; Tan, Y.; Fu, G. C.; Peters, J. C. A Mechanistic Investigation of the Photoinduced, Copper-Mediated Cross-Coupling of an Aryl Thiol with an Aryl Halide. *Chem. Sci.* **2016**, *7* (7), 4091–4100. https://doi.org/10.1039/c5sc04709a.

(71) Ahn, J. M.; Ratani, T. S.; Hannoun, K. I.; Fu, G. C.; Peters, J. C. Photoinduced, Copper-Catalyzed Alkylation of Amines: A Mechanistic Study of the Cross-Coupling of Carbazole with Alkyl Bromides. *J. Am. Chem. Soc.* **2017**, *139* (36), 12716–12723. https://doi.org/10.1021/jacs.7b07052.

(72) Kainz, Q. M.; Matier, C. D.; Bartoszewicz, A.; Zultanski, S. L.; Peters, J. C.; Fu, G. C. Asymmetric Copper-Catalyzed C-N Cross-Couplings Induced by Visible Light. *Science* **2016**, *351* (6274), 681–684. https://doi.org/10.1126/science.aad8313.

(73) Ng, Y. Y.; Tan, L. J.; Ng, S. M.; Chai, Y. T.; Ganguly, R.; Du, Y.; Yeow, E. K. L.; Soo, H. Sen. Spectroscopic Characterization and Mechanistic Studies on Visible Light Photoredox Carbon-Carbon Bond Formation by Bis(Arylimino)Acenaphthene Copper Photosensitizers. *ACS Catal.* **2018**, *8* (12), 11277–11286. https://doi.org/10.1021/acscatal.8b02502.

(74) Kee, J. W.; Ng, Y. Y.; Kulkarni, S. A.; Muduli, S. K.; Xu, K.; Ganguly, R.; Lu, Y.; Hirao, H.; Soo, H. S. Development of Bis(Arylimino)Acenaphthene (BIAN) Copper Complexes as Visible Light Harvesters for Potential Photovoltaic Applications. *Inorg. Chem. Front.* **2016**, *3* (5), 651–662. https://doi.org/10.1039/c5qi00221d.

(75) Kancherla, R.; Muralirajan, K.; Sagadevan, A.; Rueping, M. Visible Light-Induced Excited-State Transition-Metal Catalysis. *Trends Chem.* **2019**, *1* (5), 510–523. https://doi.org/10.1016/j.trechm.2019.03.012.

(76) Li, C.; Kong, X. Y.; Tan, Z. H.; Yang, C. T.; Soo, H. Sen. Emergence of Ligand-to-Metal Charge Transfer in Homogeneous Photocatalysis and Photosensitization. *Chem. Phys. Rev.* **2022**, *3* (2), 021303. https://doi.org/10.1063/5.0086718.

(77) Shen, D.; Saracini, C.; Lee, Y. M.; Sun, W.; Fukuzumi, S.; Nam, W. Photocatalytic Asymmetric Epoxidation of Terminal Olefins Using Water as an Oxygen Source in the Presence of a Mononuclear Non-Heme Chiral Manganese Complex. *J. Am. Chem. Soc.* **2016**, *138* (49), 15857–15860. https://doi.org/10.1021/jacs.6b10836.

(78) Nuhant, P.; Oderinde, M. S.; Genovino, J.; Juneau, A.; Gagné, Y.; Allais, C.; Chinigo, G. M.; Choi, C.; Sach, N. W.; Bernier, L.; Fobian, Y. M.; Bundesmann, M. W.; Khunte, B.; Frenette, M.; Fadeyi, O. O. Visible-Light-Initiated Manganese Catalysis for C−H Alkylation of Heteroarenes: Applications and Mechanistic Studies. *Angew. Chem. Int. Ed.* **2017**, *56* (48), 15309–15313. https://doi.org/10.1002/anie.201707958.

(79) Long, W.; Lian, P.; Li, J.; Wan, X. Mn-Catalysed Photoredox Hydroxytrifluoromethylation of Aliphatic Alkenes Using CF3SO2Na. *Org. Biomol. Chem.* **2020**, *18* (33), 6483–6486. https://doi.org/10.1039/d0ob01322f.

(80) Wang, L.; Lear, J. M.; Rafferty, S. M.; Fosu, S. C.; Nagib, D. A. Ketyl Radical Reactivity via Atom Transfer Catalysis. *Science* **2018**, *362* (6411), 225–229. https://doi.org/10.1126/science.aau1777.

(81) Liang, Y.-F.; Steinbock, R.; Yang, L.; Ackermann, L. Continuous Visible-Light Photoflow Approach for a Manganese-Catalyzed (Het)Arene C−H Arylation. *Angew. Chem. Int. Ed.* **2018**, *57* (33), 10785–10789. https://doi.org/10.1002/ange.201805644.

(82) Kern, J.; Chatterjee, R.; Young, I. D.; Fuller, F. D.; Lassalle, L.; Ibrahim, M.; Gul, S.; Fransson, T.; Brewster, A. S.; Alonso-Mori, R.; Hussein, R.; Zhang, M.; Douthit, L.; de Lichtenberg, C.; Cheah, M. H.; Shevela, D.; Wersig, J.; Seuffert, I.; Sokaras, D.; Pastor, E.; Weninger, C.; Kroll, T.; Sierra, R. G.; Aller, P.; Butryn, A.; Orville, A. M.; Liang, M.; Batyuk, A.; Koglin, J. E.; Carbajo, S.; Boutet, S.; Moriarty, N. W.; Holton, J. M.; Dobbek, H.; Adams, P. D.; Bergmann, U.; Sauter, N. K.; Zouni, A.; Messinger, J.; Yano, J.; Yachandra, V. K. Structures of the Intermediates of Kok's Photosynthetic Water Oxidation Clock. *Nature* **2018**, *563* (7731), 421–425. https://doi.org/10.1038/s41586-018-0681-2.

(83) Yatabe, T.; Tokunaga, T.; Matsumoto, T.; Kikkawa, M.; Yoon, K. S.; Ogo, S. A MnI Model for the Photoinhibited Species of Oxygen-Evolving Complex. *Chem. Lett.* **2018**, *47* (1), 34–36. https://doi.org/10.1246/cl.170869.

(84) Barman, M. K.; Jana, A.; Maji, B. Phosphine-Free NNN-Manganese Complex Catalyzed α-Alkylation of Ketones with Primary Alcohols and Friedländer Quinoline Synthesis. *Adv. Synth. Catal.* **2018**, *360* (17), 3233–3238. https://doi.org/10.1002/adsc.201800380.

(85) Wang, J.; Ganguly, R.; Yongxin, L.; Díaz, J.; Soo, H. Sen; García, F. Synthesis and the Optical and Electrochemical Properties of Indium(III) Bis(Arylimino)Acenaphthene Complexes. *Inorg. Chem.* **2017**, *56* (14), 7811–7820. https://doi.org/10.1021/acs.inorgchem.7b00539.

(86) Hong, Z.; Chong, W. K.; Ng, A. Y. R.; Li, M.; Ganguly, R.; Sum, T. C.; Soo, H. Sen. Hydrophobic Metal Halide Perovskites for Visible-Light Photoredox C−C Bond Cleavage and Dehydrogenation Catalysis. *Angew. Chem. Int. Ed.* **2019**, *58* (11), 3456–3460. https://doi.org/10.1002/anie.201812225.

(87) Lim, J. H.; Engelmann, X.; Corby, S.; Ganguly, R.; Ray, K.; Soo, H. Sen. C-H Activation and Nucleophilic Substitution in a Photochemically Generated High Valent Iron Complex. *Chem. Sci.* **2018**, *9* (16), 3992–4002. https://doi.org/10.1039/c7sc05378a.

(88) Ng, L. K. S.; Tan, E. J. C.; Goh, T. W.; Zhao, X.; Chen, Z.; Sum, T. C.; Soo, H. Sen. Mesoporous SiO 2 /BiVO 4 /CuO x Nanospheres for Z-Scheme, Visible Light Aerobic C–N Coupling and Dehydrogenation. *Appl. Mater. Today* **2019**, *15*, 192–202. https://doi.org/10.1016/j.apmt.2019.01.010.

(89) Kenyon, R. L., Wiesner, J. A., Kwartler, C. E. Chloroquine manufacture. *Ind. Eng. Chem. Res.*, **1949**, *41* (4), 654-662. https://pubs.acs.org/doi/pdf/10.1021/ie50472a002.

(90) Patra, K.; Laskar, R. A.; Nath, A.; Bera, J. K. A Protic Mn(I) Complex Based on a Naphthyridine- N -Oxide Scaffold: Protonation/Deprotonation Studies and Catalytic Applications for Alkylation of Ketones . *Organometallics* **2022**, *41* (14), 1836–1846. https://doi.org/10.1021/acs.organomet.2c00085.

(91) Robles, O.; Romo, D. Chemo-and Site-Selective Derivatizations of Natural Products Enabling Biological Studies. *Nat. Prod. Rep.* **2014,** *31* (3), 318-334. https://doi.org/10.1039/c3np70087a.

(92) Hasdenteufel, F.; Luyasu, S.; Hougardy, N.; Fisher, M.; Boisbrun, M.; Mertes, P.-M.; Kanny, G. Structure-Activity Relationships and Drug Allergy. *Curr. Clin. Pharmacol.* **2012**, *7* (1), 15–27. https://doi.org/10.2174/157488412799218815.

(93) McKinney, J. D.; Richard, A.; Waller, C.; Newman, M. C.; Gerberick, F.; Hasdenteufel, F.; Luyasu, S.; Hougardy, N.; Fisher, M.; Boisbrun, M.; Mertes, P.-M.; Kanny, G.; Robles, O.; Romo, D. The Practice of Structure Activity Relationships (SAR) in

Toxicology. *Toxicol. Sci.* **2000**, 56 (1), 8–17. https://doi.org/10.1039/c3np70087a.

(94) Levy, J. N.; Alegre-Requena, J. V.; Liu, R.; Paton, R. S.; McNally, A. Selective Halogenation of Pyridines Using Designed Phosphine Reagents. *J. Am. Chem. Soc.* **2020**, *142* (25), 11295–11305. https://doi.org/10.1021/jacs.0c04674.

(95) Margolis, B. J.; Long, K. A.; Laird, D. L. T.; Ruble, J. C.; Pulley, S. R. Assembly of 4-Aminoquinolines via Palladium Catalysis : A Mild and Convenient Alternative to SNAr Methodology. *J. Org. Chem.* **2007**, *72* (6), 2232–2235. https://doi.org/10.1021/jo062168u.

(96) Yamakawa, T.; Matsukura, H.; Nomura, Y., Yoshika, M.; Masaki, M.; Igata, H.; Okabe, S. Synthesis and structure-activity relationships of N-substituted 2-[(2-imidazolylsulfinyl)methyl]anilines as a new class of gastric hydrogen/potassium ion-ATPase inhibitors. *Chem. Pharm. Bull.* **1991**, *39* (7), 1746–1752. https://doi.org/10.1248/cpb.39.1746.

(97) Huang, Z.; Guan, R.; Shanmugam, M.; Bennett, E. L.; Robertson, C. M.; Brookfield, A.; McInnes, E. J. L.; Xiao, J. Oxidative Cleavage of Alkenes by O2with a Non-Heme Manganese Catalyst. *J. Am. Chem. Soc.* **2021**, *143* (26), 10005–10013. https://doi.org/10.1021/jacs.1c05757.

(98) Mansour, A. M.; Friedrich, A. The CO Release Properties of K2: N 1, N 2 Mn(i) Tricarbonyl PhotoCORMs with Tridentate Benzimidazole Coligands. *Inorg. Chem. Front.* **2017**, *4* (9), 1517–1524. https://doi.org/10.1039/c7qi00390k.

(99) Khaled, R. M.; Friedrich, A.; Ragheb, M. A.; Abdel-Ghani, N. T.; Mansour, A. M. Cytotoxicity of Photoactivatable Bromo Tricarbonyl Manganese(i) Compounds against Human Liver Carcinoma Cells. *Dalton Trans.* **2020**, *49* (27), 9294–9305. https://doi.org/10.1039/d0dt01539c.

(100) Jamatia, R.; Mondal, A.; Srimani, D. Visible-Light-Induced Manganese-Catalyzed Reactions: Present Approach and Future Prospects. *Adv. Synth. Catal.* **2021**, *363* (12), 2969–2995. https://doi.org/10.1002/adsc.202100151.

(101) Costa, R.O.; Ferreira, S.S.; Pereira, C.A.; Harmer, J.R.; Noble, C.J.; Schenk, G.; Franco, R.W.; Resende, J.A.; Comba, P.; Roberts, A.E.; Fernandes, C.; Horn Jr, A. A New Mixed-Valence Mn(II)Mn(III) Compound With Catalase and Superoxide Dismutase Activities. *Front. Chem.* **2018**, *6*, 491. https://doi.org/10.3389/fchem.2018.00491.

(102) Wang, Z.; Hao, Y.; Qiang, H.; Xu, C.; Chen, C. Facile synthesis of nitrogen-doped mesoporous hollow carbon nanospheres@ NiCo2O4 for high-performance supercapacitors. *Ionics* **2021**, *27* (1),:315-323. https://doi.org/10.1007/s11581-020-03794-0.

(103) Mo, Z.; Xu, H.; Chen, Z.; She, X.; Song, Y.; Lian, J.; Zhu, X.; Yan, P.; Lei, Y.; Yuan, S.; Li, H. Construction of MnO2/Monolayer g-C3N4 with Mn vacancies for Z-scheme overall water splitting. *Appl Catal. B* **2019**, *241*, 452-460. https://doi.org/10.1016/j.apcatb.2018.08.073.

(104) Tang, W.; Wu, X.; Li, D.; Wang, Z.; Liu, G.; Liu, H.; Chen, Y. Oxalate route for promoting activity of manganese oxide catalysts in total VOCs' oxidation: effect of calcination temperature and preparation method. *J. Mater. Chem. A* **2014**, *2* (8), 2544-2554. https://doi.org/10.1039/C3TA13847J.

(105) Hastuti, E.; Subhan, A.; Amonpattaratkit, P.; Zainuri, M.; Suasmoro, S. The effects of Fe-doping on MnO2: phase transitions, defect structures and its influence on electrical properties. *RSC Adv*., **2021**, *11* (14), 7808-7823. https://doi.org/10.1039/D0RA10376D.

(106) Li, X. X.; Lee, Y. M.; Nam, W. Manganese complex-catalyzed oxidation and oxidative kinetic resolution of secondary alcohols by hydrogen peroxide. *Chem. Sci.* **2017**, *8* (11), 7476-7481. https://doi.org/10.1039/C7SC00891K.

TOC:

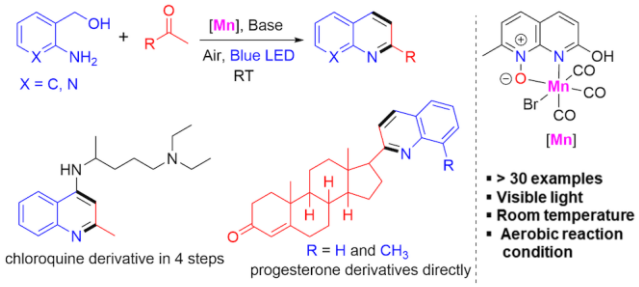
OH
NH2
X = C, N
[Mn], Base
Air, Blue LED
RT
R
HN
N
chloroquine derivative in 4 steps
H
H
H
O
R = H and CH3
progesterone derivatives directly
OH
CO
Mn
Br
CO
CO
[Mn]
▪ > 30 examples
▪ Visible light
▪ Room temperature
▪ Aerobic reaction condition